HEFAT2012
9th International Conference on Heat Transfer, Fluid Mechanics and Thermodynamics
16 – 18 July 2012
Malta

COMPARISON OF HEAT FLUX SENSORS FOR INTERNAL COMBUSTION ENGINES ON TWO HOT AIR GUN TEST RIGS AND A TEST ENGINE

Cornelis, K. [a], Van Caelenberg, R. [a], Demuynck J.*[,a], De Paepe M.[a], Chana K.S.[b] and Verhelst S.[a]
*Author for correspondence
[a] Department of Flow, Heat and Combustion Mechanics,
Ghent University - UGent,
Gent, 9000, Belgium
[b] Department of Engineering Science,
University of Oxford,
Oxford, OX1 3PJ, United Kingdom
E-mail: joachim.demuynck@ugent.be

ABSTRACT

The heat transfer that occurs in the cylinder of internal combustion engines has a great influence on the efficiency, power output and emissions. Development of a model that is able to predict the heat transfer is needed in order to be able to use simulations for optimization of these three properties. Prior to developing a model, the heat transfer phenomenon has to be thoroughly investigated by performing measurements inside an engine. This allows for a detailed understanding of the process and for a validation of model predictions. In previous works, a commercially available thermopile has been used to measure the heat transfer in a hydrogen combustion engine. The use of this sensor as a heat flux sensor has already been positively evaluated in a previous paper. Its dimensions, however, limit its usability for engine measurements, as it is too large to mount in production type engines. Therefore, a comparison with two alternative sensors was performed to select the best one for engine heat transfer research. Two variations of a calibration rig were used, one with a fast opening shutter and one with a chopper with adjustable speed. This paper presents a comparison of the rise time based on measurements on both test rigs. Furthermore, measurements were carried out on a test engine to evaluate the capability of the sensors to determine the heat transfer to the cylinder walls.

INTRODUCTION

The current energy issues clearly demonstrate the need for alternative and renewable fuels such as hydrogen, alcohols and biological oils. As these fuels all have one or more properties that differ from those of conventional fuels, it is expected that the heat transfer inside the engine, which greatly influences the efficiency, power output and emissions, also shows different characteristics. In order to be able to use simulations for the design and optimization of engines that run on these alternative fuels, it is necessary to develop a heat transfer model that is able to correctly predict the heat transfer that occurs. Recent studies [1, 2] have shown that the most frequently used heat transfer models, such as those of Annand [3] and Woschni [4], are not able to predict the heat transfer that occurs during combustion of hydrogen. Even for conventional fuels, the results are not accurate. This shows that the heat transfer process is not yet completely understood. For the development of a new model, it is necessary to investigate the heat transfer mechanisms, in particular the convective and radiant heat transfer from the combustion gases to the inner cylinder walls. We are investigating the heat transfer in hydrogen and methanol combustion engines, focusing on convection since radiation is negligible in spark ignition engines [5].

To characterize the heat transfer process inside the cylinder, it is necessary to measure the transient heat flux at the gas-wall interface. In literature, the heat flux is most of the time calculated from transient surface temperature measurements using a signal processing technique. We, on the other hand, have always used a commercial thermopile sensor for our research [6, 7], as it has been calibrated by the manufacturer to directly convert the output voltage into heat flux.

Because of the large outer dimensions (diameter type 8.74 mm), this sensor cannot be mounted inside a production type engine. So, in order to be able to perform measurements in different types of engines, it is necessary to select an alternative sensor. Therefore, this paper compares the rise time of three different sensors: the thermopile, a thin film gauge temperature sensor and an eroding ribbon K-type temperature sensor.

NOMENCLATURE

Abbreviations

EVO	*exhaust valve opening*
HFM	*heat flux microsensor*
HFS	*heat flux sensor*

RTD		*resistance temperature detector*
RTS		*resistance temperature sensing*
TFG		*thin film gauge*
TP	$J/Km^2s^{1/2}$	*thermal product*
TDC		*top dead center*

Greek symbols

α_0	$\Omega/°C$	*temperature coefficient of TFG*
ρ	kg/m^3	*density*

Roman Symbols

h		*impulse response*
k	*W/mK*	*thermal conductivity*
q	W/cm^2	*heat flux*
T	*°C*	*temperature*
T_0	*°C*	*ambient temperature*
V_0	*V*	*voltage over TFG at* T_0
x	*m*	*distance*

EXPERIMENTAL METHOD

Sensors and signal processing

The reference sensor was an uncoated Vatell HFM-7 sensor, as shown in Figure 1. This sensor was used before to measure the heat flux inside a hydrogen combustion engine [6, 7]. The sensor has two output signals: a heat flux signal from a thermopile (HFS-signal) and a temperature signal from an RTD (RTS-signal). The Vatell AMP-6 amplifier was used as a current source for the RTD and as an amplifier for both output signals. The sensor was calibrated up to 40 W/cm^2 by Vatell and polynomials were given to calculate the heat flux directly out of the HFS- and RTS-signal (see HFM manual [8]).

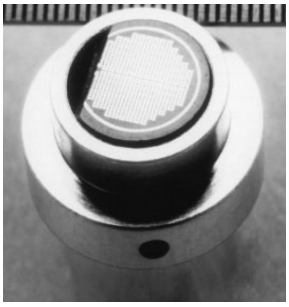

Figure 1 uncoated HFM-7 sensor

The first alternative sensor was developed at the University of Oxford to measure the heat flux inside gas turbines [9]. The sensor (TFG: thin film gauge) is a thin film RTD and is used to measure the surface temperature of a substrate. The TFG was deposited directly on a Macor substrate, as schematically shown in Figure 2. Two of these TFG sensors were placed on the surface of a bolt in order to mount them on the calibration rig. Below the surface, a K-type thermocouple is located.

The relationship between the resistance and the temperature of the TFG is given in the following equation, with R_0 being the resistance at a reference temperature T_0:

$$R = R_0.[1 + \alpha_0.(T - T_0)] \quad (1)$$

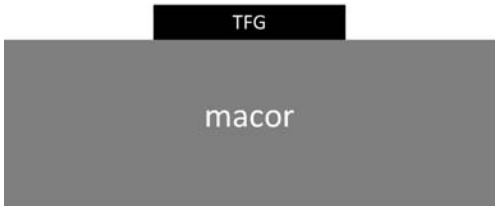

Figure 2 TFG on Macor

A constant current was sent through the TFG to generate a change in the voltage over the sensor proportional to the change of the sensor's resistance in function of the temperature. Multiplying the equation above with the current I results in the following equation, which is used to derive the temperature increase out of the measured voltage increase (V_0 is the measured voltage at T_0):

$$\Delta T = \frac{\Delta V}{\alpha_0 V_0} \quad (2)$$

The temperature coefficient, α_0, was retrieved from calibration experiments in an oven. The temperature in the oven was controlled by a reference Pt-100 thermocouple and varied between 25°C and 80°C in 7 steps. After stabilisation of the oven, the resistance of the TFG was measured. The measurements for one of the TFG's are given in Figure 3. The least squares method was used to generate a linear curve through the measured points. This curve was converted into the form of equation 1 in order to calculate α_0. In order to do this, T_0 has to be chosen as the ambient temperature in the lab, which was 24.3°C. The calculated coefficients are presented in Table 1.

Table 1: temperature coefficients of the TFG sensors

Sensor	α_0 (mΩ/°C)
TFG1 on Macor	1.98 +/- 0.04
TFG2 on Macor	2.02 +/- 0.04

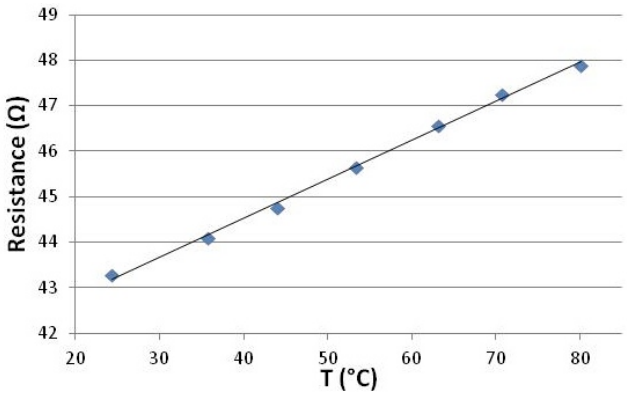

Figure 3 resistance as function of temperature for TFG1

The second alternative sensor is a standard eroding ribbon K-type temperature sensor, constructed by Nanmac. The sensor output was converted into a temperature signal by using the standard polynomial for K-type thermocouples.

For both alternative sensors, a signal processing technique was used to convert the measured temperature trace into a heat flux trace. Here, the impulse response method developed at the University of Oxford [10] was used. This method assumes that the sensor is a linear time invariant system with the temperature being the input and the heat flux being the output as shown in Figure 4.

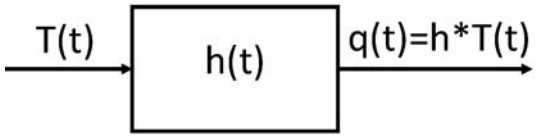

Figure 4 the heat flux is the convolution of the impulse response and the temperature

The system is characterised by its impulse response h(t) which can be used to calculate the output from the input with the convolution integral:

$$q(t) = h(t) * T(t) = \int_{-\infty}^{\infty} h(\tau)T(t-\tau)d\tau \qquad (3)$$

Because discrete signals are recorded, the convolution integral is converted into a summation:

$$q[n] = \sum_{k=0}^{N-1} h[k] \cdot T[n-k] \qquad (4)$$

The impulse response has to be calculated once for each sensor according to the methods described in [10]. This allows a fast heat flux calculation once the impulse response filter has been designed. The impulse response of the TFG on Macor and the eroding ribbon is that of a semi-infinite gauge with one layer. The material property that is needed for the calculation of the impulse response is the thermal product (TP), being equal to $\sqrt{\rho \cdot c_p \cdot k}$. For the TFG, the TP of Macor is required, which was determined experimentally at Oxford, together with its relative error [9]. For the eroding ribbon, the physical properties were approximated by using the values for the material surrounding the junction, AISI 304 stainless steel, as it is expected that this material has the greatest influence on the thermal properties of the sensor. The value of the TP was determined by looking up physical properties of similar materials in ref. [11]. The relative error was based on the spread of the thermal properties found in literature. The thermal products are presented in Table 2.

All measurements were performed using a National Instruments PXI system connected to a measurement computer.

Table 2: thermal products of the materials used

Material	TP ($J/m^2Ks^{1/2}$)	Relative error on TP (%)
Macor	2050	4.2
AISI 304 Stainless Steel	7697	20

Hot air-gun test rig

The first part of the experiments was conducted on a 'hot-air-gun test rig'. This rig is an improved version of the rig previously used in ref. [13]. The rig can be adjusted in order to perform two kinds of measurements: a single heat flux step can be measured by using a shutter and multiple heat flux steps are measured by using a chopper, powered by an electrical motor. The heat flux generated by the shutter and chopper is shown in Figure 5.

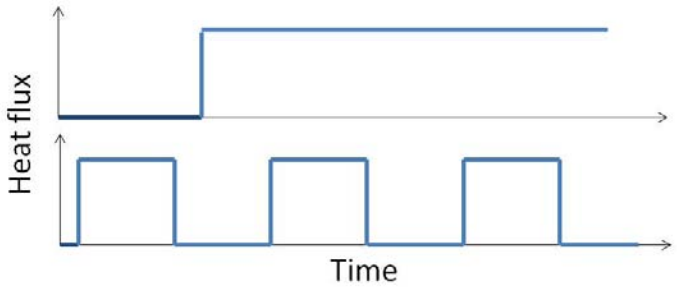

Figure 5 Heat flux generated by shutter (upper) and chopper (lower)

When the chopper is used, the speed of the electrical motor can be varied in order to determine the influence on the rise time and evaluate the dynamic behaviour of the sensor. The basic rig consists out of two structures that are not connected to each other, as shown in Figure 6.

The sensors and heat gun are mounted on the first structure. The heat gun is pointed upwards so that natural and forced convection work in the same direction. This way, higher heat fluxes can be achieved. All the sensors are mounted inside or on a bolt in order to fix them on the test rig. On the second structure, the rail with the fast-opening shutter is mounted. When using the chopper, this is mounted as shown in Figure 7. Measurements were performed on one sensor at a time.

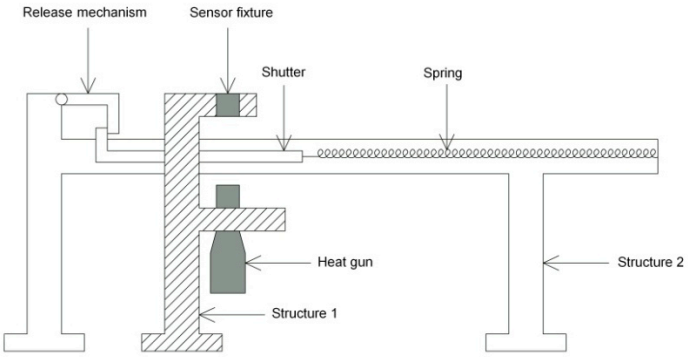

Figure 6 the hot-air-gun test rig

Figure 7 chopper rig

Rise time calculation

The rise time was calculated using a self-developed method, which can be explained by looking at Figure 8. A measurement is accepted when the first peak, marked by the red rhombus, is located above the mean flux level of the step, which is shown by the red line. If the measurement is accepted, the rise time is calculated between two points located at 10 and 95% of the mean flux level. These points are marked by the green triangles.

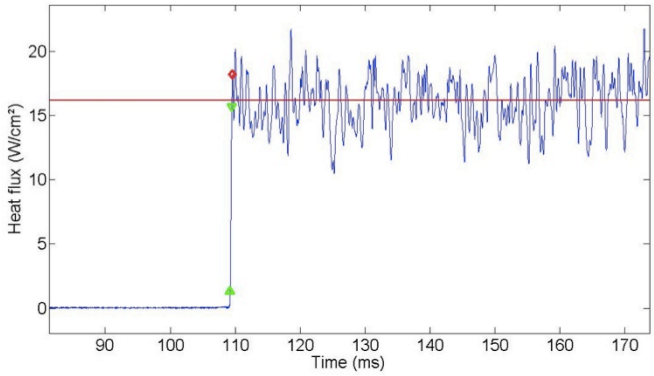

Figure 8 Rise time calculation method – HFM measurement

Error Analysis

In order to determine the relative heat flux error, a thorough error analysis was conducted using the methods described in [14]. The results can be found in Table 3. The high relative error for the eroding ribbon is caused by the high uncertainty on the thermal properties of the sensor.

Table 3: relative heat flux errors

Sensor	Relative heat flux error (%)
HFM	3
TFG	13
Eroding Ribbon	23

CFR engine

To further evaluate the performance of the different sensors, measurements were carried out on a CFR (Cooperative Fuel Research) engine. The engine is operated at a constant speed of 600 rpm and is equipped with one gas injector in the intake manifold that is used for the injection of methane. As can be seen on Figure 9, the engine is easy accessible so the sensors can be mounted in three different positions (P2-P4). The spark plug is mounted in position P1.

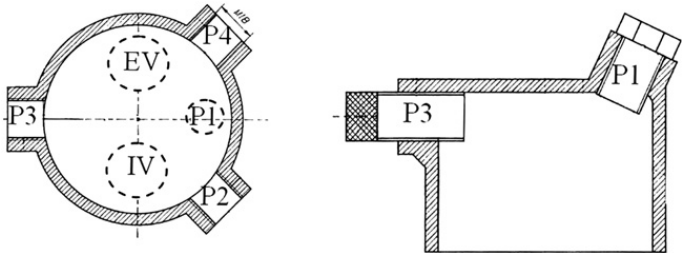

Figure 9 Cross-section of the CFR engine, P1: spark plug, P2-P4: sensor positions, IV: inlet valve, EV: exhaust valve

Measurements were performed on two different engine settings, which can be found in Table 4.

Table 4 measurements used for evaluation

Measurement	λ	IGN	Throttle position	CR
1	1	24 °CA BTDC	87°	8.67
2	1	24 °CA BTDC	75°	8.67

RESULTS AND DISCUSSION

Shutter rig measurements

Heat flux traces of the measurements performed with the HFM, TFG (only one is shown) and eroding ribbon are shown in Figure 10. Due to the high noise level, the measured voltages of the TFG and the eroding ribbon were filtered with a 5th order Butterworth-filter with a cut-off frequency of 4000 Hz and 2000 Hz, respectively.

For each measurement, the heat gun was turned on some time before opening the shutter so the nominal heat flux level was reached. Between measurements, the sensors were cooled down to ambient temperature.

The shutter speed was calculated using the method described in [13] and was found to be 7.88 m/s (+/- 1.27 m/s).

The different start-times of the heat flux steps are caused by the varying opening speed of the shutter and the release mechanism. However, this does not pose any problems for the rise time calculation. When comparing the three traces, it is clear that the heat gun does not provide a very stable heat flux signal. Moreover, the rise time of each of the sensors also shows some fluctuations. Therefore, it is only possible to compare the sensors based on an average rise time and average heat flux level. It is clear that the eroding ribbon is subject to a great amount of noise. This noise is not caused by the heat gun, as it is also present when the shutter is closed, which is not the case for the HFM and the TFG.

The mean heat flux levels were calculated for each sensor. The results are shown in Figure 11. The rise time was calculated for each heat flux trace and the average rise time and standard deviation were calculated for each sensor. These results are shown in Figure 12.

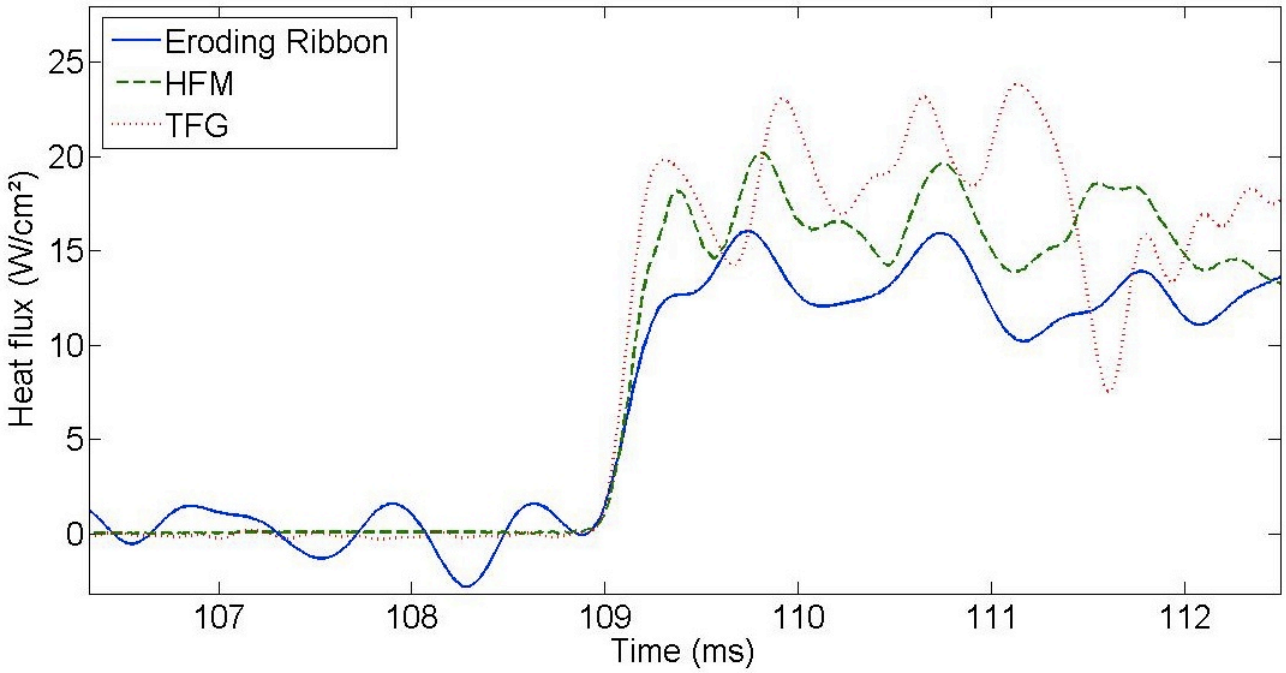

Figure 10 heat flux traces for shutter rig

We can conclude that the mean heat flux levels measured by the HFM and the eroding ribbon are the same. It seems that the TFG sensors measure a slightly higher heat flux level, but the spread on the measurements is too large for this to be significant. Furthermore, we see that the TFG's and the HFM have the same rise time, which is significantly lower than that of the eroding ribbon.

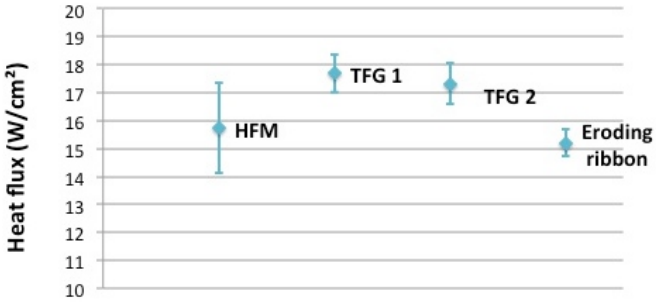

Figure 11 mean heat flux levels for the shutter rig

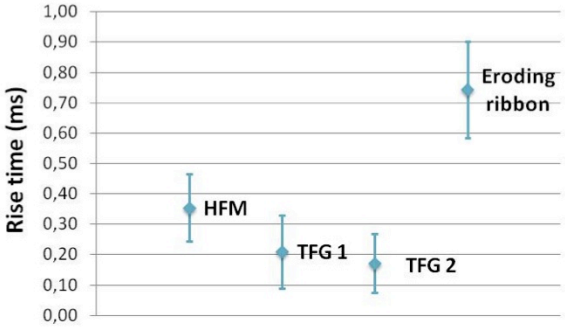

Figure 12 rise time results for the shutter rig

Chopper rig measurements

Measurements were performed on different speeds of the chopper. Before measuring, the heat gun was turned on to allow for the sensor to reach a steady state temperature. Each measurement contains several cycles. For each sensor, a cycle measured at a speed of 1000 rpm is shown in Figure 13. Because the heat flux levels did not correspond between the three sensors, the traces are plotted as a percentage of the nominal level. For the discussion about this non-correspondence, see the paragraph about engine measurements.

For the calculation of the mean rise time, 10 measurements were used. The results are shown in Figure 14, using the same criterion as for the shutter rig measurements. Because the rise time of both the TFG sensors did not differ on the shutter rig, it was calculated for only one of them.

The flux applied to the sensors can be divided into a transient and a steady state part. For the TFG and the eroding ribbon, the heat flux was calculated with the impulse response method from the surface temperature signal. However, this only results in the transient part of the heat flux. To obtain the total heat flux the steady state part has to be calculated using the 1D Fourier equation, given by

$$q = -k\frac{\Delta T}{\Delta x} \tag{5}$$

Thus, a second thermocouple measurement at a depth Δx beneath the surface of the sensor is needed. The TFG is equipped with such a sensor and the heat flux shown in Figure 13 consists of the sum of the transient and steady state heat flux. The eroding ribbon, however, is not equipped with such a sensor. As a result, the trace shown is the transient heat flux after shifting the lower portion to zero in order to be able to perform the rise time calculations.

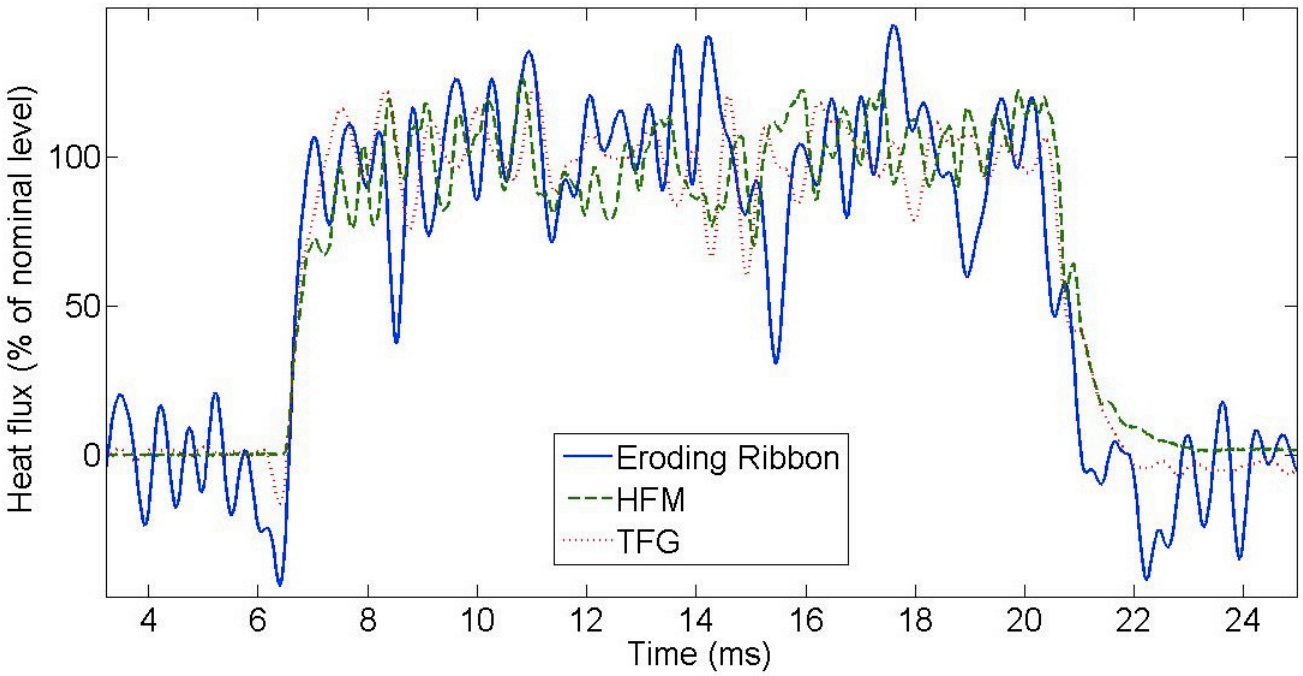

Figure 13 heat flux traces for chopper rig

From Figure 14, it can be concluded that the rise time of the different sensors does not differ significantly. We can also see that there is no influence of the motor speed.

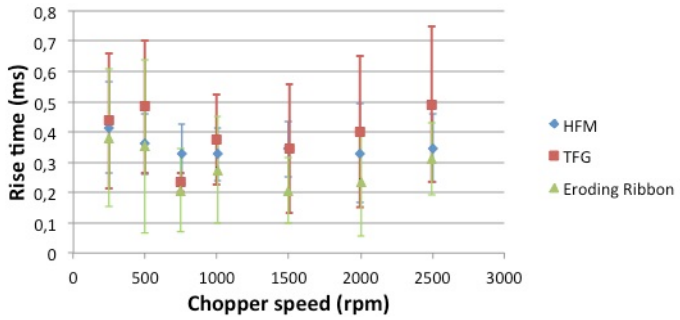

Figure 14 rise time results for the chopper rig

It was calculated that a chopper speed of 818 rpm (+/- 132 rpm) corresponds with the shutter opening speed. If we look at the average rise times on the shutter rig and those at 750 rpm on the chopper rig, we see that there is no significant difference for the HFM and the TFG's, but that the rise time of the eroding ribbon is slightly higher on the shutter rig. This leads to the conclusion that the eroding ribbon performs better, in terms of rise time, at higher temperatures, while the other sensors maintain the same performance regardless of their temperature.

Engine measurements

Each measurement consists of 60 engine cycles. For the HFM sensor, the flux can be directly calculated from the RTS and HFS signal. For the TFG and eroding ribbon, the impulse response method was applied to the measured surface temperature to obtain the transient part of the heat flux. To obtain the total heat flux for each cycle, it was assumed that the heat flux equals zero when the difference between the gas temperature, calculated from the cylinder pressure, and the surface temperature is zero. Thus, for each cycle, the transient heat flux from the impulse response method is shifted to zero for this point in order to obtain the total heat flux. To cancel out cyclic variation, the heat flux was averaged over all 60 cycles.

In Figure 15, a comparison is given between the HFM and TFG sensors for measurement 1 in position P4. The general shape of the heat flux signal corresponds quite well. After exhaust valve opening both sensors measure an increase in heat flux, which is caused by the hot combustion gases passing by the sensor that is located close to the exhaust valve. For the peak fluxes, an error bar is plotted that illustrates the relative error of the heat flux. It is clearly visible that the peak fluxes do not correspond well, since the error bars of the two peaks do not overlap.

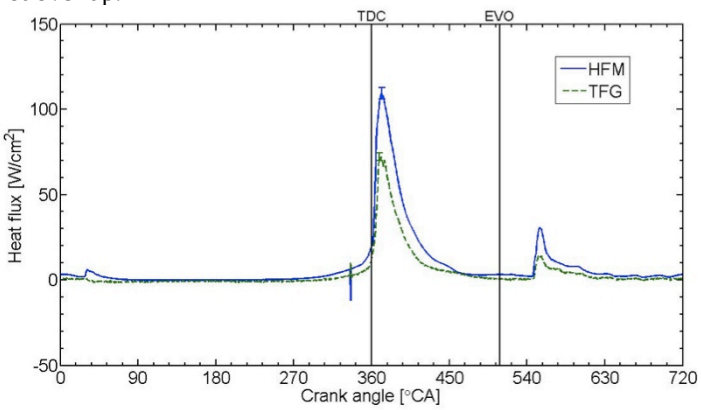

Figure 15 heat flux comparison between HFM and TFG for measurement 1 in position P4

Two possible causes can be attributed to these findings. First, the linear behaviour of the TFG resistance versus temperature as shown in Figure 3 could change to a non-linear relationship at higher temperatures. This has yet to be verified. Second, a change in thermal properties at higher temperatures can give rise to higher thermal products and thus results in an increase in calculated heat flux.

In Figure 16, a comparison between the HFM and the eroding ribbon is shown for the two measurements in position P2. Error bars are plotted to illustrate the relative error on the peak heat flux. For both measurements, the heat flux calculated from the eroding ribbon temperature measurement is too high. This leads to the conclusion that the approximation of the thermal product is incorrect for elevated temperatures.

Buttsworth [12] remarks that several materials can have an influence on the sensor response to a given heat flux. The impulse response method, however, does not allow for these materials to be taken into account. During engine measurements, it might be that not only the material surrounding the junction influences the overall behaviour of the sensor. A calibration method that allows for the thermal properties to be determined at elevated temperatures has yet to be developed.

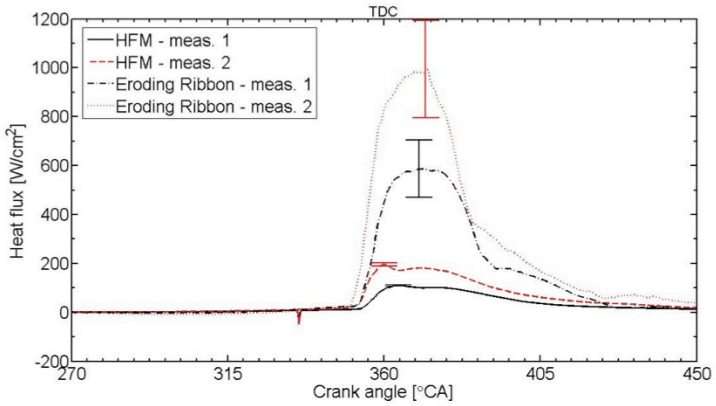

Figure 16 heat flux comparison between HFM and Eroding Ribbon for two measurements in position P2

Sensor evaluation

In order to select an alternative for the HFM, several properties have to be evaluated. An overview can be found in Table 5.

Table 5: sensor evaluation

	HFM	TFG	Eroding Ribbon
Rise time	+	+	+
Accuracy	+	o	-
Robustness	+	+	-
Signal processing	++	+	-
Dimensions	--	+	-

The rise time ranking was based on the measurements performed on both rigs. The sensor accuracy refers to the relative heat flux error calculated on the shutter rig. The robustness of the eroding ribbon is lower than that of the other sensors because the junctions have to be renewed from time to time in order to achieve low rise times. Furthermore, the HFM allows for easy processing thanks to the polynomials provided by Vatell. The TFG can be processed using the impulse response method thanks to the depth thermocouple, which is not present in the eroding ribbon. Finally, the major drawback of the HFM is its size. The TFG is much smaller and offers possibilities for easier mounting.

CONCLUSIONS

We have always used a commercially available thermopile sensor (HFM) for the heat flux measurements in a hydrogen combustion engine. Its large dimensions, however, make it impossible to mount in a production engine. Therefore, this paper has provided a comparison of the HFM with two alternative sensors: a thin film gauge (TFG) temperature sensor and an eroding ribbon K-type temperature sensor. In order to compare the sensors, the following criteria were used: rise time, accuracy, robustness, signal processing and sensor dimensions. The rise time comparison is based on measurements performed on two calibration rigs: a shutter rig and a chopper rig.

The results show some limitations of the alternative sensors and the processing method used. There is a large relative error on the eroding ribbon measurements because of the high uncertainty on the approximated thermal properties. This approximation was necessary to be able to use the impulse response method. Engine measurements have shown that this approximation leads to inaccurate results, thus emphasizing the need for a calibration method.

Furthermore, it was impossible to calculate the steady state heat flux for the eroding ribbon measurements because of the absence of a thermocouple beneath the surface. Therefore, it was impossible to compare heat flux levels on the chopper rig.

Engine measurements show that further research for the thermal properties of the TFG and the eroding ribbon sensors at elevated temperatures is necessary in order to be able to process engine measurements.

This paper shows that the TFG is the best alternative for the HFM sensor. The sensor and its thermal properties, however, have to be calibrated at elevated temperatures in order be able to use it for engine measurements.

ACKNOWLEDGEMENTS

The authors of this paper would like to acknowledge the suggestions and technical assistance of Koen Chielens, Patrick De Pue and Trevor Godfrey. The authors gratefully acknowledge the Institute for the Promotion of Innovation through Science and Technology in Flanders (IWT-Vlaanderen) for the Ph.D. grant SB-81139 and the Research Foundation - Flanders (FWO) for the Research Grant 1.5.147.10N.

REFERENCES

1. Demuynck, J., et al., *On the applicability of empirical heat transfer models for hydrogen combustion engines.* International Journal of Hydrogen Energy, 2011. **36**(1): p. 975-984.

2. Shudo, T. and H. Suzuki, *Applicability of heat transfer equations to hydrogen combustion.* JSAE Review, 2002. **23**(3): p. 303-308.
3. Annand, W.J.D., *Heat transfer in the cylinders of reciprocating internal combustion engines*. Proc Instn Mech Engrs, 1963. **177**(36): p. 973-996.
4. Woschni, G. (1967) *A Universally Applicable Equation for the Instantaneous Heat Transfer Coefficient in the Internal Combustion Engine*.
5. Borman, G.L. and K. Nishiwaki, *Internal-Combustion Engine Heat-Transfer.* Progress in Energy and Combustion Science, 1987. **13**(1): p. 1-46.
6. Demuynck, J., et al., *Investigation Of The Influence Of Engine Settings On The Heat Flux In A Hydrogen- And Methane-Fuelled Spark Ignition Engine*. Applied Thermal Engineering, 2011. **31**: p. 1220-1228.
7. Demuynck, J., et al., *Local heat flux measurements in a hydrogen and methane spark ignition engine with a thermopile sensor.* International Journal of Hydrogen Energy, 2009. **34**(24): p. 9857-9868.
8. Vatell. *Heat Flux Microsensor manual*. 2010; Available from: http://www.vatell.com/hfm.htm.
9. Piccini, E., S.M. Guo, and T.V. Jones, *The development of a new direct-heat-flux gauge for heat-transfer facilities.* Measurement Science and Technology, 2000. **11**(4): p. 342-349.
10. Oldfield, M.L.G., *Impulse response processing of transient heat transfer gauge signals.* Journal of Turbomachinery-Transactions of the ASME, 2008. **130**(2).
11. Key to Metals AG. *Key to Metals Database*. 2012; Available from: http://www.keytometals.com.
12. Buttsworth, D.R., R. Stevens, and C.R. Stone, *Eroding ribbon thermocouples: impulse response and transient heat flux analysis.* Measurement Science and Technology, 2005. **16**(7): p. 1487-1494.
13. Demuynck, J., et al. *Rise Time Evaluation of the Heat Flux Microsensor (HFM) on Hot Air-Gun Test Rig*. in *8th International Conference on Heat Transfer, Fluid Mechanics and Thermodynamics*. 2011. Pointe Aux Piments, Mauritius.
14. Taylor, J.R., *An introduction to error analysis: the study of uncertainties in physical measurements*. 1982: University Science Books.